Sorption Mechanisms of Zinc to Calcium Silicate Hydrate: X-ray Absorption Fine Structure (XAFS) Investigation

ARTICLE *in* ENVIRONMENTAL SCIENCE AND TECHNOLOGY · MAY 2001

Impact Factor: 5.33 · DOI: 10.1021/es001437+ · Source: PubMed

5 AUTHORS, INCLUDING:

C. Annette Johnson
Eawag: Das Wasserforschungs-Institut des E…
77 PUBLICATIONS **3,424** CITATIONS
SEE PROFILE

Rainer Dähn
Paul Scherrer Institut
60 PUBLICATIONS **890** CITATIONS
SEE PROFILE

Erich Wieland
Paul Scherrer Institut
101 PUBLICATIONS **2,086** CITATIONS
SEE PROFILE

Environ. Sci. Technol. **2001**, *35,* 1550−1555

Sorption Mechanisms of Zinc to Calcium Silicate Hydrate: X-ray Absorption Fine Structure (XAFS) Investigation

FELIX ZIEGLER,*,† ANDRÉ M. SCHEIDEGGER,‡ C. ANNETTE JOHNSON,† RAINER DÄHN,‡ AND ERICH WIELAND‡

Department of Resource and Waste Management, EAWAG, Swiss Federal Institute of Environmental Science and Technology, CH-8600 Dübendorf, Switzerland, and Waste Management Laboratory, PSI, Paul Scherrer Institute, CH-5232 Villigen PSI, Switzerland

In this study, X-ray absorption fine structure (XAFS) spectroscopy has been used to further elucidate the binding mechanisms of Zn(II) to calcium silicate hydrate (C-S-H), the quantitatively most important cement mineral. Such knowledge is essential for the assessment of the long-term behavior of cement-stabilized waste materials. XAFS spectra of the Zn(II) equilibrated with C-S-H(I) for up to 28 days are best modeled by tetrahedral coordination of Zn(II) by four O atoms in the first atomic shell. Beyond the first coordination shell, data analysis of more highly concentrated samples suggests the presence of two distinct Zn distances and possibly the presence of an Si shell. On the basis of the comparison with a set of reference compounds, this coordination environment can be reasonably related to the structure of hemimorphite, a naturally occurring zinc silicate, and/or the presence of γ-$Zn(OH)_2$. At the lowest Zn uptake, the above fitting approach failed and data could be described best with a Zn−Si and a Zn−Ca shell. Previous work has been able to show that Zn(II) diffuses into the C-S-H(I) particles and does not form discrete precipitates, so the findings appear to confirm the incorporation of Zn(II) in the interlayer of C-S-H(I).

Introduction

Cement is commonly used worldwide for the stabilization and solidification of waste materials containing heavy metal species (*1*). However, due to their high heavy metal content, these cement-based waste materials remain a potential environmental risk over centuries (*2*−*4*), whereas the emissions may last thousands of years. Thus, the long-term leachability of the cement-stabilized residues is the most important factor in the assessment of the potential hazards associated with their landfilling (*5*). To assess the long-term mobility of heavy metals in landfill systems, it is necessary to understand the binding mechanisms of the heavy metals in the cement matrix. The binding mechanisms that have been discussed in the literature include surface complex formation, ion exchange, solid−solution formation, and (surface-)precipitation of pure and mixed mineral phases (*6*−*11*). Among the different cement minerals, calcium silicate hydrate (C-S-H) is a prime candidate for heavy metal binding because of its abundance and appropriate structure (*12*).

Several authors have examined the interaction of Zn with cement minerals and especially C-S-H: Under certain conditions, calcium zincate [$CaZn_2(OH)_6$] appears to be formed, probably via surface precipitation at the cement particles (*13*), but there is also evidence that this is an intermediate phase, which is no longer detectable after a few days (*14*), and the subsequent incorporation of Zn into C-S-H is described (*15*). On the basis of studies with crystalline calcium silicates, cation exchange reactions of Zn with Ca are also proposed to occur in poorly crystalline or amorphous C-S-H phases (*16*, *17*). In a recent study, Moulin et al. (*18*) suggested, on the basis of sorption isotherm and ^{29}Si NMR measurements, that structural retention by Si−O−Zn bonds is involved in the sorption of Zn to C-S-H. From an examination of the solubility of coprecipitates of C-S-H(I) and Zn, Johnson and Kersten (*19*) postulated a solid−solution mechanism for the Zn sorption to C-S-H. Ziegler et al. (*20*) used a combination of kinetics, sorption experiments, and microscopic measurements and reported the diffusion of Zn into the C-S-H(I) particles. They postulated an incorporation of Zn in the interlayer of the C-S-H structure. All of these studies are not able to finally determine the dominant sorption mechanism of Zn to C-S-H on a molecular level. However, incorporation of Zn into C-S-H appears to be likely.

The present study tries to further elucidate the binding mechanisms of Zn to C-S-H by using X-ray absorption fine structure (XAFS). XAFS is able to detect the local coordination of Zn and thus provide structural information on Zn sorbed to C-S-H. Samples that had been equilibrated for short and longer periods and coprecipitation samples were compared. Zn reference minerals were examined as possible structural models for Zn sorbed to C-S-H. A C-S-H species called C-S-H(I) was chosen. It is considerably more ordered than the C-S-H formed in ordinary cement pastes. Different investigations showed it to be a structurally imperfect form of 1.4-nm tobermorite (*21*−*23*), a natural cement mineral with a layer structure similar to that of 2:1 clay minerals.

Experimental Methods

Materials. To prevent CO_2 contamination, all procedures involving alkaline solutions and solids were performed in a glovebox in an argon atmosphere with a $p_{CO_2} < 1$ ppm. Solutions were generally prepared using boiled ultrapure water (Barnstead Nanopur, 17 MW). All solid samples were freeze-dried, analyzed for their crystalline phase composition by X-ray powder diffraction (XRPD), and stored in desiccators above NaOH pellets.

The synthesis of C-S-H(I) was performed after the method of Atkins et al. (*24*) to achieve a C-S-H(I) with a Ca/Si ratio of 1. For the subsequent experiments, only the size fraction of C-S-H(I) particles <63 μm was used. Calcium zincate [$Zn_2Ca(OH)_6 \cdot 2H_2O$] was prepared after the method of Sharma (*25*). Zinc orthosilicate (Willemite, Zn_2SiO_4) and smithsonite ($ZnCO_3$) were synthesized after methods from Brauer (*26*). γ-Zinc hydroxide was prepared after the method of Christensen (*27*). Hemimorphite [$Zn_4Si_2O_7(OH)_2 \cdot H_2O$] was provided by the Institute of Mineralogy and Petrography at ETH Zürich (sample 1830.3.5).

Samples of Zn sorbed to C-S-H(I) were prepared at 1, 19, and 190 μM total Zn concentrations and equilibration times of 30 min and 28 days. Because of the high solubility

* Corresponding author telephone: +41-1-8173150; fax: +41-1-8235210; e-mail: zieglerlang@dplanet.ch.
† EAWAG.
‡ PSI.

10.1021/es001437+ CCC: $20.00

Published on Web 03/07/2001

of C-S-H(I) and to avoid changes in the stoichiometry of C-S-H(I), the sorption experiments needed to be carried out in suspensions that had been pre-equilibrated with respect to C-S-H(I). Thus, 156.9 mg of C-S-H(I) was added to 4000 mL of the pre-equilibrated solution ([OH^-] = 8.3 mM, [Ca] = 3.0 mM, [Si] = 0.10 mM, [NaCl] = 100 mM) in 5000-mL HDPE bottles. After 7 days of equilibration, 200 mL of appropriate Zn stock solutions was slowly added and equilibrated. The samples have Zn contents corresponding to a molar Si/Zn ratio in the solid phase from 0.0014 (1 μM−30 min), 0.019, and 0.031 (19 μM−30 min and −28 days) to 0.28 and 0.29 (190 μM−30 min and −28 days). Further details of the sorption experiments are described in ref *20*.

Two coprecipation samples were produced as follows: A Zn-C-S-H(I) coprecipitate was produced according to the method of Johnson and Kersten (*19*), resulting in a solid with a molar fraction of Zn in the solid phase of 0.1. For a Zn−Si coprecipitate, 100 mL of a Si standard solution (1000 ppm of Si, 5 M OH^-) was mixed in a 250-mL HDPE centrifuge beaker with 3.5 mL of a Zn stock solution (1.0 M Zn, 0.1 M H^+), resulting in a solution with a molar Si/Zn ratio of 1.0. To coprecipitate Zn and Si, concentrated HCl (50 mL) was added, resulting in a pH of ~11.5. The precipitate was aged for 24 h. It was amorphous as determined by XRPD.

X-ray Absorption Fine Structure (XAFS) Spectroscopy. *Sample Preparation*. The Zn-treated C-S-H(I) samples as well as the coprecipitation samples were pressed into the 5 × 15 mm slit of 3-mm-thick Teflon sample holders and sealed with Mylar film. The reference samples were intensively ground in an agate mortar, and 1.0 g of the powder was diluted with 9.0 mg of Hoechst wax C micropowder (Merck). A portion (150 mg) of the mixture was pressed to tablets of 3-mm thickness and 13-mm diameter. The tablets were taped on a Teflon sample holder prior to the Zn-XAFS measurements.

Data Collection. XAFS spectra were recorded at beamline BM1B (Swiss-Norwegian beamlines, SNBL) at the European Synchrotron Radiation Facility (ESRF, Grenoble, France). An Si (111) channel-cut monochromator was used. Beam energy was calibrated by assigning the first inflection on the K absorption edge of a Zn metal foil to an energy of 9.659 keV.

The spectra of the sorption and coprecipitation samples were collected in fluorescence mode using a Stern-Heald-type detector (Lytle detector, The EXAFS Co.). The spectra of the reference samples were collected in transmission mode using ionization chambers. Fill gases used were Ar for the Lytle detector and N_2 for the I_0 and I_T detectors. To prevent CO_2 contamination, the samples were placed in an aluminum chamber equipped with Kapton windows, which was continuously purged with N_2 during the measurements. The chamber was connected to a reservoir with liquid N_2 to collect the spectra at 77 K. Comparisons of spectra recorded at 77 K and room temperature revealed no change in structural information, whereas the signal-to-noise ratio was maximized by dampening thermal disorder. All scans were collected at least in triplicate and averaged to improve the signal-to-noise ratio.

Data Analysis. Data reduction was performed using WinXAFS 97 1.1 following standard procedures (*28*). The resulting $\chi(k)$ functions were weighted by k^3 to account for the dampening of oscillations with increasing k and Fourier transformed to achieve radial structure functions (RSF). A Bessel window with a smoothing parameter of 3 was used to suppress artifacts due to the finite Fourier filtering range between 3.6 and 12.9 Å (except the sorption sample with the lowest Zn concentrations, at which data analysis was limited to 10.0 $Å^{-1}$). Theoretical scattering paths for the fit were calculated with FEFF 7.02 (*29*), using the structure of hemimorphite. The accuracies of the derived structural parameters were estimated from the reference minerals by a comparison of the experimental data with literature values. Thus, the accuracies for the interatomic distance (R) are $\Delta R = \pm 0.01 - 0.02$ Å for the first shell and $\Delta R = \pm 0.03 - 0.05$ Å for the second shell. For the coordination number (N) it is $\Delta N = \pm 30\%$.

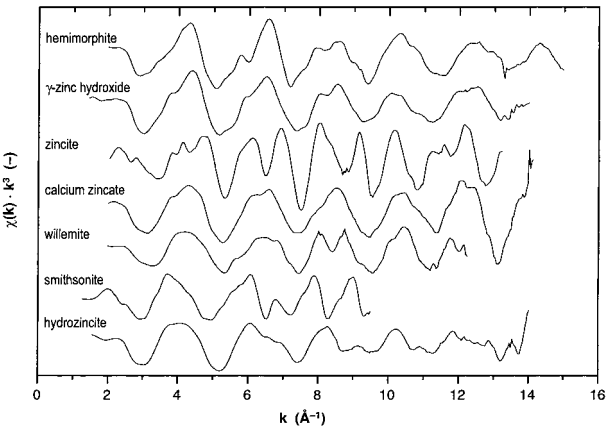

FIGURE 1. Normalized, background-subtracted, and k^3-weighted Zn-XAFS spectra (χ-function) of the reference compounds.

Results

Reference Minerals. To discuss the structural origin of the XAFS data of the Zn sorption samples, we have measured a set of reference compounds. The normalized, background-subtracted, and k^3-weighted Zn-XAFS spectra of the reference compounds are shown in Figure 1. All of the spectra of the reference compounds show characteristic structural details and in some cases a strong beat pattern.

The quantitative analyses of the spectra are summarized in Table 1. Except for the spectrum of hydrozincite, all spectra could be fitted reasonably. Zn atoms with different coordination environment (tetrahedral and octahedral) are present within the structure (*30*), making data analysis of hydrozincite complex. Thus, data of this mineral will not be discussed further.

As a comparison to the XAFS analyses, literature data on the structural parameters of the corresponding reference minerals as determined by XRD are also shown in Table 1. For the first coordination sphere, there is generally a good coincidence between data derived from XAFS measurements and from the literature. Some difficulties exist in the fitting of the second coordination sphere, mainly of γ-zinc hydroxide, calcium zincate, and willemite. The interatomic distances for the second Zn−Zn shell in γ-zinc hydroxide and the Zn−Si shell of willemite are too short (3.37 Å compared to 3.50 and 3.57 Å, and 2.98 Å compared to 3.10−3.23 Å). Additionally, the coordination numbers are too low (0.8 and 0.5 compared to 2 and 4). In the spectrum of calcium zincate, it appears to be impossible to fit a Zn−Zn shell at the appropriate distance of ~3.44 Å. Such observations could be explained either by a strong disorder of the neighboring atoms at these distances, which makes them invisible in the XAFS spectra, or by the presence of impurities influencing the XAFS spectra.

A literature review of papers on Zn-XAFS reveals that this behavior is not unusual for Zn minerals. O'Day et al. (*31*) measured some Zn reference compounds (hydrozincite, smithsonite, willemite, γ- and ϵ-zinc hydroxide, and zincite). They remarked that the derived interatomic distances for the two zinc hydroxides did not match distances from structure determinations by XRPD. The results for the other compounds were not reported. Generally, only few Zn-XAFS studies can be found in the literature, and the derived structures for reference compounds such as zincite, zinc

TABLE 1. Structural Parameters of the Reference Compounds Derived from Zn-XAFS Analysis and from the Literature: Phase Shift (ΔE_0, eV), Shells, Interatomic Distances (R, Å), Coordination Numbers (N), and Debye−Waller Factors ($\Delta\sigma^2$, Å $\times$ 10^{-3})

		first coordination sphere						second coordination sphere						
						literature values						literature values		
sample	ΔE_0	shell	R	N	$\Delta\sigma^2$	R	N	shell	R	N	$\Delta\sigma^2$	R	N	ref
hemimorphite	−1.0	Zn−O	1.93	3.8	2.9	1.94−1.98	4	Zn−Si	3.05	3.0[a]	13	3.04, 3.11, 3.20	3	*32*
								Zn−Zn	3.23	2.0[a]	6.1	3.30, 3.30	2	
								Zn−Zn	3.37	2.0[a]	6.4	3.42	2	
γ-zinc hydroxide	1.5	Zn−O	1.94	4.0[a]	3.6	1.89−2.03	4	Zn−Zn	3.24	1.5	10[a]	3.30 3.50, 3.58	2	*27*
								Zn−Zn	3.37	0.8	10[a]		2	
zincite	6.4	Zn−O	1.81	1.0[a]	0.8	1.80	1	Zn−Zn	3.19	12.0[a]	11	3.21	6	*33*
			1.98	3.0[a]	0.6	2.04	3					3.25	6	
calcium zincate	−0.2	Zn−O	1.92	3.5	2.0	1.92−1.98	4	Zn−Zn				3.44	2	*34*
								Zn−Ca	3.78	2.0[a]	9	3.78, 3.79	2	
								Zn−Zn	3.99	1.0[a]	9	4.01	1	
willemite	2.4	Zn−O	1.93	4.0[a]	6.6	1.95	4	Zn−Si	2.98	0.5	7.1	3.10−3.23	4	*35*, *36*
								Zn−Zn	3.12	1.0[a]	2.9	3.11	1	
								Zn−Zn	3.24	3.0[a]	6.4	3.21−3.24	3	
smithsonite	1.2	Zn−O	2.06	6.3	14[a]	2.11	6	Zn−C	2.97	6.0[a]	4.9	2.96	6	*37*
								Zn−O	3.19	6.0[a]	4.1	3.23	6	
								Zn−Zn	3.65	6.0[a]	9.8	3.67	6	
								Zn−C				3.76	2	
								Zn−O	3.89	6.0[a]	3.6	3.97	6	

[a] Fixed parameters during fitting procedure.

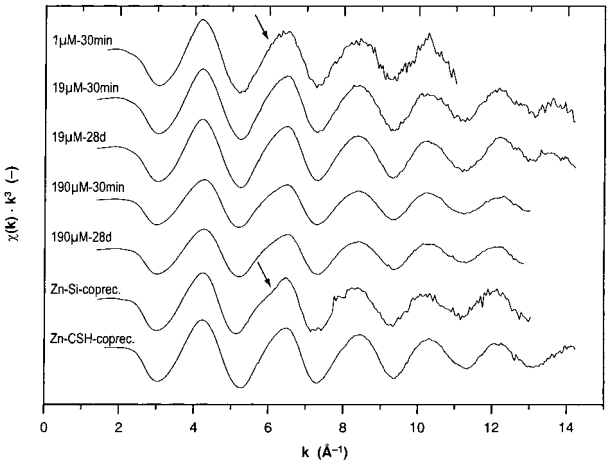

FIGURE 2. Normalized, background-subtracted, and k^3-weigthed Zn-XAFS spectra (χ-function) of Zn-treated C−S−H(I) and coprecipitation samples.

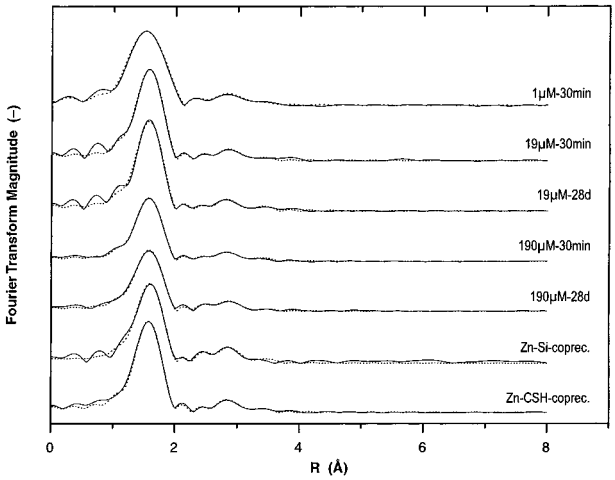

FIGURE 3. RSF obtained by Fourier transformation of the XAFS spectra shown in Figure 2. The solid lines represent the experimental data, and the dotted lines are the best multishell fits to the data (both uncorrected for phase shift).

hydroxide, and smithsonite are almost not reported. Because of the flexibility of the coordination structure of Zn, XAFS spectra of Zn minerals are difficult to fit. Furthermore, the presence of (amorphous) impurities in some of the reference minerals (γ-zinc hydroxide, calcium zincate, willemite, and smithsonite) cannot be excluded. Some reference compounds used are not commercially available and had to be synthesized for this study. The phase composition of the resulting minerals was determined by XRPD. Because the XRPD method is only able to identify crystalline phases with a content of >5%, the presence of impurities and amorphous compounds influencing the XAFS data cannot be excluded.

Sorption and Coprecipitation Samples. The normalized, background-subtracted, and k^3-weighted Zn-XAFS spectra of the sorption and the coprecipitation samples are shown in Figure 2. The different sorption samples have similar $\chi(k^3)$ functions and are all in phase. Furthermore, the spectra do not suggest any significant changes with reaction time and with increasing initial Zn concentration. In addition, the spectra from sorption samples are almost identical to the two coprecipitation samples. The spectra are dominated by a single strong sinusoidal oscillation. Between 5 and 7 $Å^{-1}$ a clear deviation from a single sinusoidal oscillation becomes apparent, as indicated by arrows. A capped oscillation is observed, and it seems to be directly related to the Zn concentration in the sample.

Fourier transformations of the spectra in Figure 2 yield RSFs. RSF aids the identification of characteristic frequencies resulting from backscattering atoms coordinated with the absorbing Zn atoms. Figure 3 shows the RSFs of the different samples and the respective best fits that result from multishell fitting. The spectra are uncorrected for phase shift. Qualitative analyses of the RSF spectra do not reveal any significant differences between the samples equilibrated under different conditions, as already pointed out for the normalized spectra ($\chi \cdot k^3$). All spectra show a main peak at $R \approx 1.6$ Å, which corresponds to the signal from the first coordination shell of Zn. Further peaks are present in the region between 2.2 and 3.5 Å. The intensities of the peaks are small. Nevertheless, the intensities are significantly above the background (noise level between, e.g., 5 and 8 Å), clearly suggesting the presence of structure beyond the first coordination shell.

TABLE 2. Structural Parameters of the Sorption and Coprecipitation Samples Derived from Zn-XAFS Analysis: Phase Shifts (ΔE_0, eV), Residuals (%), Interatomic Distances (R, Å), Coordination Numbers (N), Debye−Waller Factors ($\Delta\sigma^2$, Å^2 × 10^{-3}), and Contribution

			Zn−O shell				Zn−Si shell				Zn−Zn(1) shell				Zn−Zn(2) shell			
sample	ΔE_0	residual[a]	R	N	$\Delta\sigma^2$	contrib	R	N	$\Delta\sigma^2$	contrib	R	N	$\Delta\sigma^2$	contrib	R	N	$\Delta\sigma^2$	contrib
19 μM−30 min	0.8	7.5	1.94	3.9	4.9	100	2.99	0.2	5[b]	4	3.26	0.6	5[b]	15	3.39	0.4	5[b]	9
19 μM−28 days	1.4	8.2	1.94	4.3	4.4	100	2.92	0.2	5[b]	4	3.23	0.9	5[b]	21	3.38	0.8	5[b]	17
190 μM−30 min	1.6	3.7	1.94	3.1	4.7	100	2.94	0.3	5[b]	6	3.23	0.8	5[b]	25	3.38	0.7	5[b]	20
190 μM−28 days	2.0	5.7	1.94	3.2	5.0	100	2.98	0.4	5[b]	9	3.27	0.8	5[b]	26	3.42	0.5	5[b]	15
Zn−Si-coprec	1.8	8.6	1.96	4.2	5.0	100	3.00	0.8	5[b]	13	3.29	1.5	5[b]	13	3.44	1.1	5[b]	36
Zn−CSH-coprec	0.6	5.2	1.94	4.4	4.6	100	2.97	0.1	5[b]	2	3.25	0.8	5[b]	17	3.38	0.6	5[b]	12
hemimorphite	0.2	14.6	1.93	3.8	2.1	100	3.03	1.8	5[b]	26	3.28	2.3	5[b]	49	3.42	1.8	5[b]	33

			Zn−O shell				Zn−Si shell				Zn−Ca shell			
sample	ΔE_0	residual[a]	R	N	$\Delta\sigma^2$	contrib	R	N	$\Delta\sigma^2$	contrib	R	N	$\Delta\sigma^2$	contrib
1 μM−30 min	1.5	9.0	1.94	4.0[b]	3.7	100	3.08	0.8	5[b]	11	3.81	0.7	5[b]	8

			Zn−O shell				Zn−Si shell				Zn−Zn shell			
sample	ΔE_0	residual[a]	R	N	$\Delta\sigma^2$	contrib	R	N	$\Delta\sigma^2$	contrib	R	N	$\Delta\sigma^2$	contrib
1 μM−30 min	1.4	10.3	1.94	4.0[b]	3.7	100	3.02	0.7	12[b]	9	3.32	0.5	5[b]	10

			Zn−O shell				Zn−Si(1) shell				Zn−Si(2) shell			
sample	ΔE_0	residual[a]	R	N	$\Delta\sigma^2$	contrib	R	N	$\Delta\sigma^2$	contrib	R	N	$\Delta\sigma^2$	contrib
1 μM−30 min	1.5	10.0	1.94	4.0[b]	3.7	100	3.08	0.6	5[b]	9	3.55	0.9	5[b]	9

[a] Deviation between experimental data and fit given by the relative residual in percent. N represents the number of data points, and y_{exp} and y_{theor} are the experimental and theoretical data points, respectively. %Res = $\{[N\sum i=1|\ y_{exp}(i) - y_{theor}(i)|]/N\sum i=1 y_{exp}(i)\} \times 100$. [b] Fixed parameters during fitting procedure.

The structural parameters derived from Zn-XAFS analysis are summarized in Table 2. The quantitative analyses reveal that in the first coordination shell, Zn is surrounded by four O atoms. The determined Zn−O bond distance ($R \approx 1.94$ Å) is typical of Zn in tetrahedral coordination with O. Literature values are in the range of 1.8−2.0 Å (see Table 1), whereas in compounds with octahedral coordination of Zn with O (e.g., smithsonite and hydrozincite), the bond distance is significantly larger, in the range of 2.0−2.1 Å. The Zn−O bond distance does not appear to be affected by the different equilibration conditions of the samples. For the second coordination sphere different models have been evaluated and compared to fit the experimental data of the different samples. For this reason, the second coordination shell contribution (2.6−3.7 Å) was Fourier backtransformed. Figure 4 illustrates the Fourier-filtered and backtransformed spectrum of the second coordination sphere from the 190 μM−30 min sample. The experimental spectrum (solid line) is shown together with the fits with one and two Zn shells and two Zn shells and one Si shell, that is, shells consisting of Zn or Si atoms at different distinct distances from the central Zn atom. The fits with one Zn shell are generally poor: they are out of phase at higher distances, and the magnitude fits only in the intermediate k range. The fits with two Zn shells are much better. For the first Zn shell with the significantly higher contribution to the spectrum, the distance to the central Zn atom is slightly shorter (≈3.25 Å) than for the fit with only one Zn shell (3.27 Å). The second Zn shell has a smaller contribution and is located at ∼3.4 Å. The phase of the two Zn shell fit correctly reflects the experimental data, but at low and high distances, the magnitude is too low. For most samples, the best fits are obtained by fitting three shells to the second coordination sphere, two Zn shells and one Si shell. As can be seen in Figures 3 and 4, this approach allowed us to successfully model the experimental data.

Data analysis suggests that the first Zn shell is at a distance of 3.23−3.29 Å and contains one or two Zn atoms (N = 0.6−1.5). The second Zn shell contributes less to the total spectrum (N = 0.4−1.1) than the first shell and is located at distances between 3.38 and 3.44 Å. The Si shell is located at distances between 2.92 and 3.0 Å. The coordination number ranges from 0.2 to 0.8; therefore, the contribution of this shell to the spectrum is generally low and, thus, the presence of the Si shell is questionable.

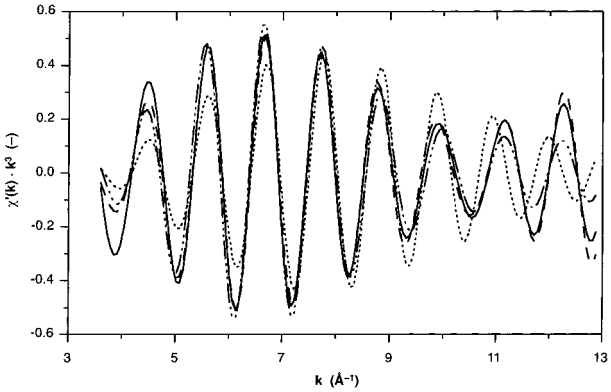

FIGURE 4. Fourier-filtered Zn-XAFS spectrum of the second coordination sphere (2.6−3.7 Å) after the backtransformation into k space (sample 190 μM−30 min). The solid line indicates the Fourier-filtered experimental data, the dotted line shows the fit with one Zn shell, the dash−dotted line shows the fit with two Zn shells, and the dashed line shows the fit with two Zn shells and one Si shell.

No trends toward higher coordination numbers appear to exist for higher Zn content or longer equilibration time of the samples. This lack of any significant differences in the spectra of most samples indicates that either Zn is located in a similar coordination environment for all samples or, if additional Zn phases are formed with increasing Zn content of the samples, they have to be completely disordered and therefore do not contribute to the XAFS spectra.

The sorption sample with the lowest Zn concentrations (1 μM−30 min) behaves differently in the fitting procedures of the second coordination sphere, and the fitting approach

selected for the more highly concentrated samples failed. We evaluated three different combinations of shells to fit the spectrum at low Zn concentration: combinations of one Si shell and one Ca shell or one Si shell and one Zn shell or two Si shells. In the first solution (Si and Ca), the observed distances (3.08 and 3.81 Å) are typical for edge sharing of the ZnO_4 tetrahedron with the SiO_4 tetrahedron and the CaO_6 octahedron, respectively. Please note that similar Zn−Si and Zn−Ca distances can be observed in Zn reference compounds (Table 1). The second fit solution (Si and Zn) appears to be related to the solutions for the samples with higher Zn concentrations. However, it differs insofar as only one Zn shell is observed at a Zn−Zn distance (3.33 Å) intermediate to the two Zn−Zn distances observed for the more concentrated samples. The third fit solution yielded two Zn−Si shells at distances of 3.08 and 3.55 Å. Although the shorter Zn−Si distance is in the range of Zn−Si distances in zinc silicate compounds, this is not the case for the longer Zn−Si distance. Table 2 reveals that the fit solution with Si and Ca is slightly better (Res = 9.0%) than the fit solutions with Zn and Si (Res = 10.3%) and two Si shells (Res = 10.0%).

We have also evaluated fits with a Zn−Si shell and a Zn−Ca-shell or two Zn−Si shells for the more concentrated samples. However, the fit quality clearly degraded in all cases. For example, for the 190 μM−28 day sample, the residual increased from 5.7 to 11.1% when the data were fitted with a Zn−Si and a Zn−Ca shell instead. Thus, although the fit solution with Si and Ca works well at the lowest Zn concentration, it can be excluded with a fair degree of confidence for the samples with higher concentrations.

Discussion

The first coordination sphere of the sorption and coprecipitation samples clearly indicates a tetrahedral coordination of Zn with O. This excludes smithsonite as a structural model because the Zn atoms are octahedrally coordinated by O atoms in this structure. An exchange of Ca by Zn in the structure of C-S-H(I) can be excluded as well, because Ca is coordinated by six or seven O atoms.

The second coordination sphere of more highly concentrated Zn sorption and coprecipitation samples can be fitted with two Zn shells and most probably one Si shell. The Zn−Zn distances are characteristic, and with this zincite, calcium zincate and willemite can be excluded as structural models: Willemite does not fit because the Zn−Zn distances are too short compared to the sorption and coprecipitation samples (3.12 and 3.24 Å compared to 3.26 and 3.40 Å). Calcium zincate is not suitable because the Zn−Zn distances of the second Zn shell are too large (4.03 Å) and Ca could not be detected in the second shell of the more highly concentrated Zn sorption and coprecipitation samples. The Zn−Zn distances in zincite are too short (R = 3.19 Å instead of R = 3.23−3.44 Å).

The Zn−Zn distances can be explained only by a structure as in hemimorphite and γ-zinc hydroxide. For the following reasons, we hypothesize that hemimorphite appears to be the most suitable structural model for the sorption and coprecipitation samples.

(i) The EXAFS spectrum of the Zn−Si coprecipitate is very similar to those of sorption samples, suggesting the presence of a similar Zn phase.

(ii) Although the Zn−Si contribution is small and questionable, Figure 3 revealed that the presence of a Zn−Si shell does improve the fits.

(iii) Hemimorphite behaves analogously to the sorption and coprecipitation samples in the fitting procedures; if the Si shell is omitted, the distances for the two Zn shells become shorter.

Table 2 reveals that the measured coordination numbers in the second coordination sphere are clearly lower for C-S-H samples compared to hemimorphite. This can be a sign for the lower ordering of the Zn environment.

Another possibility is that the samples contain a mixture of different Zn sorption modes or newly formed phases. Any attempt to model the spectra of the C-S-H samples with a linear combination of spectra from different reference compounds was not successful. Interestingly, by taking the spectrum of the sample at the lowest Zn concentrations (1 μM−30 min) and adding the hemimorphite spectrum, the spectra of the sorption samples could be successfully simulated. This approach yielded a hemimorphite contribution in the range of up to 20%. This may be an indication for changes in the Zn coordination structure toward a more hemimorphite-like structure with increasing zinc content of the samples and would explain the significantly lower Zn−Zn coordination numbers compared to hemimorphite and the fact that the fit quality degraded when the data were fit with a Zn−Si and Zn−Ca shell instead.

The nature of the structure in the sample with the lowest Zn concentration cannot be explained conclusively. Possibly, Zn is coordinated with Si and Ca groups at surfaces of the C-S-H particles.

Such a behavior would be in agreement with former investigations of Ziegler et al. (*20*). They investigated the Zn sorption to C-S-H(I) with a combination of kinetics, sorption experiments, and microscopic measurements and showed that at short equilibration times, Zn is predominantly sorbed at the surfaces of the C-S-H(I) surfaces and, afterward, Zn diffuses into the C-S-H particles. For samples with low Zn content (1 and 19 μM Zn samples) the isotherm as well as the microscopic measurements did not indicate the formation of Zn surface precipitates. On the basis of considerations about the C-S-H(I) structure, they proposed the incorporation of Zn in the interlayer of C-S-H(I) with the diffusion of Zn into the C-S-H(I) particles. They argued that this incorporation could not be a classical 1:1 isomorphous substitution of Zn at particular sites in the C-S-H(I) structure, because quantitative analysis of C-S-H(I) particles did not show any significant exchange of Zn for Ca or Si. The results from XAFS analysis with corresponding samples reveal the presence of some Si bonding in the second coordination sphere of Zn in all samples from low to high Zn content. With ZnO_4 tetrahedra present in the interlayer of C-S-H(I), a bonding to Si−O sites is feasible at two different corners of SiO_4 tetrahedra oriented toward the interlayer. Because of the stereochemical hindrance within the C-S-H(I) structure and the significantly larger ZnO_4 tetrahedron compared to a SiO_4 tetrahedron, the ZnO_4 tetrahedra can only be connected to the SiO_4 corners by slightly twisting. With this, the observed Zn−Si distances have to be smaller than the maximum theoretical Zn−Si distance of 3.56 Å derived from corner sharing of a ZnO_4 and a SiO_4 tetrahedron. This is in agreement with the XAFS data, which show Zn−Si distances of ∼3.0 Å, a common value for zinc silicate minerals. Additionally, these observations are in agreement with the data from Moulin et al. (*18*). Their isotherm measurements were accompanied by ^{29}Si NMR measurements to characterize the Zn retention sites in C-S-H(I). Their spectra showed Si lines that can be attributed to sites involving Si−O−Zn bonds. They concluded, therefore, that Zn is structurally retained by C-S-H(I), but they did not make any further conclusions about the effective sorption mechanism.

In summary, our XAFS data confirm the presence of Si−O−Zn bonds. The incorporation of Zn in the interlayer of C-S-H(I) at least partially connected to Si sites appears to be a possible mechanism for the incorporation of Zn into C-S-H(I).

Acknowledgments

We gratefully acknowledge the funding of the Swiss Federal Institute of Environmental Science and Technology (EAWAG) and the assistance and helpful discussions of friends and colleagues including Christian Ludwig, Hermann Moench, Jan Tits, and Urs Berner. We thank Dr. Peter Brack for the hemimorphite sample and Dr. Arnold Stahel for help with XRPD analysis (Institute of Mineralogy and Petrography at ETH Zürich). Furthermore, we thank the staff of BM1B (Swiss-Norwegian Beamlines, SNBL) at the ESRF in Grenoble for the support during the measurements.

Literature Cited

(1) Glasser, F. P. *J. Hazard. Mater.* **1997**, *52*, 151−170.
(2) Johnson, C. A.; Käppeli, M.; Brandenberger, S.; Ulrich, A.; Baumann, W. *J. Contam. Hydrol.* **1999**, *40*, 239−259.
(3) Ludwig, C.; Ziegler, F.; Johnson, C. A. In *Waste Materials in Construction, Putting Theory into Practice*; Goumans, J. J. J. M., Senden, G. J., van der Sloot, H. A., Eds.; Elsevier: Amsterdam, The Netherlands, 1997; pp 459−468.
(4) Ochs, M.; Stäubli, B.; Wanner, H. *Muell Abfall* **1999**, *31*, 194−205, 301−306.
(5) Baccini, P., Ed. *The Landfill: Reactor and Final Storage*; Springer: Berlin, Germany, 1989.
(6) Sprung, S.; Rechenberg, W. *Betontech. Ber.* **1988**, *38*, 193−198.
(7) Cocke, D. L. *J. Hazard. Mater.* **1990**, *24*, 231−253.
(8) Richardson, I. G.; Groves, G. W. *Cem. Concr. Res.* **1993**, *23*, 131−138.
(9) Spence, R. D., Ed. *Chemistry and Microstructure of Solidified Waste Forms*; Lewis: Boca Raton, FL, 1993.
(10) Bonen, D.; Sarkar, S. L. In *Advances in Cement and Concrete*; Grutzeck, M. W., Sarkar, S. L., Eds.; Proceedings of an Engineering Foundation Conference; American Society of Civil Engineers: New York, 1994; pp 481−498.
(11) Mollah, M. Y. A.; Vempati, R.; Lin, T.-C.; Cocke, D. L. *Waste Manage.* **1995**, *15*, 137−148.
(12) Gougar, M. L. D.; Scheetz, B. E.; Roy, D. M. *Waste Manage.* **1996**, *16*, 295−303.
(13) Cocke, D. L.; Mollah, M. Y. A. In *Chemistry and Microstructure of Solidified Waste Forms*; Spence, R. D., Ed.; Lewis: Boca Raton, FL, 1993; pp 187−242.
(14) Yousuf, M.; Mollah, A.; Vempati, R. K.; Lin, T.-C.; Cocke, D. L. *Waste Manage.* **1995**, *15*, 137−148.
(15) Lieber, W.; Gebauer, J. *Zem-Kalk-Gips* **1969**, *22*, 161−164.
(16) Komarneni, S.; Breval, E.; Roy, D. M.; Roy, R. *Cem. Concr. Res.* **1988**, *18*, 204−220.
(17) Labhsetwar, N.; Shrivastava, O. P. *React. Solids* **1989**, *7*, 225−233.
(18) Moulin, I.; Stone, W. E. E.; Sanz, J.; Bottero, J.-Y.; Mosnier, F.; Haehnel, C. *Langmuir* **1999**, *15*, 2829−2835.
(19) Johnson, C. A.; Kersten, M. *Environ. Sci. Technol.* **1999**, *33*, 2296−2298.
(20) Ziegler, F.; Gieré, R.; Johnson, C. A. *Environ. Sci. Technol.* **2001**, submitted for publication.
(21) Cong, X.; Kirkpatrick, R. J. *Adv. Cem. Based Mater.* **1996**, *3*, 144−156.
(22) Kirkpatrick, R. J.; Brown, G. E.; Xu, N.; Cong, X. *Adv. Cem. Res.* **1997**, *9*, 31−36.
(23) Kirkpatrick, R. J.; Yarger, J. L.; McMillan, P. F.; Yu, P.; Cong, X. *Adv. Cem. Based Mater.* **1997**, *5*, 93−99.
(24) Atkins, M.; Glasser, F. P.; Kindness, A. *Cem. Concr. Res.* **1992**, *22*, 241−246.
(25) Sharma, R. A. *J. Electrochem. Soc.* **1986**, *133*, 2215−2219.
(26) Brauer, G. *Handbuch der Präparativen Anorganischen Chemie*, 3rd ed.; Enke Verlag: Stuttgart, Germany, 1978; Vol. 2.
(27) Christensen, A. N. *Acta Chem. Scand.* **1969**, *23*, 2016−2020.
(28) Ressler, T. *J. Synchr. Rad.* **1998**, *5*, 118.
(29) Rehr, J. J. *FEFF: Ab initio multiple scattering X-ray absorption fine structure and X-ray absorption near edge structure code*; FEFF Project, Department of Physics, University of Washington: Seattle, WA, 1998; http://leonardo.phys.washington.edu/feff/.
(30) Ghose, S. *Acta Crystallogr.* **1964**, *17*, 1051−1057.
(31) O'Day, P. A.; Carroll, S. A.; Waychunas, G. A. *Environ. Sci. Technol.* **1998**, *32*, 943−955.
(32) Libowitzky, E.; Kohler, T.; Armbruster, T.; Rossmann, G. R. *Eur. J. Mineral.* **1997**, *9*, 803−810.
(33) Wyckoff, R. W. G. *Crystal Structures*, 2nd ed.; Interscience: New York, 1965; Vol. 1.
(34) Liebau, F.; Amel-Zadeh, A. *Krist. Tech.* **1972**, *7*, 221−227.
(35) Simonov, M. A.; Sandomirskii, P. A.; Egorov-Tismenko, Y. K.; Belov, N. V. *Sov. Phys. Dokl.* **1977**, *22*, 622−623.
(36) Simonov, M. A.; Belov, N. B. *Moscow Univ. Geol. Bull. (Engl. Transl.)* **1978**, *33*, 43−51.
(37) Effenberger, H.; Mereiter, K.; Zeman, J. *Z. Kristallogr.* **1981**, *156*, 223−243.

Received for review June 29, 2000. Revised manuscript received January 8, 2001. Accepted January 18, 2001.

ES001437+